

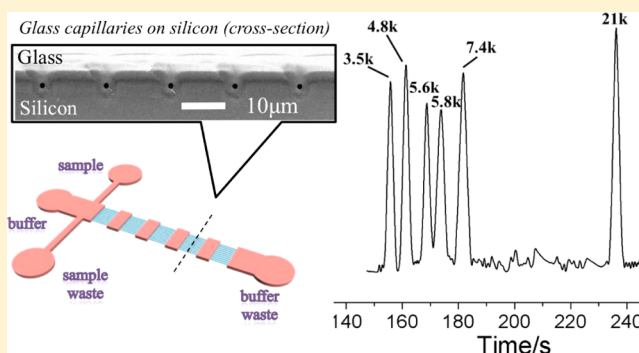
Fast DNA Sieving through Submicrometer Cylindrical Glass Capillary Matrix

Zhen Cao and Levent Yobas*

Department of Electronic and Computer Engineering, Hong Kong University of Science and Technology, Clear Water Bay, Kowloon, Hong Kong

Supporting Information

ABSTRACT: Here, we report on DNA electrophoresis through a novel artificial sieving matrix based on the highly regular submicrometer cylindrical glass capillary segments alternately arranged with wells. Such round capillaries pose a higher-order confinement resulting in a lower partition coefficient and greater entropic energy barrier while limiting the driving field strength to a small fraction of the applied electric field. In return, the separation can be performed at high average field strengths (up to 1.6 kV/cm) without encountering the field-dependent loss of resolving power. This leads to fast DNA sieving as demonstrated here on the capillaries of 750 nm in diameter. The 600 bp to 21 kbp long chains are shown to resolve within 4 min after having undergone a fairly limited number of entropic barriers (128 in total). The capillary matrix also exhibits a critical field threshold below which DNA bands fail to launch, and this occurs at a considerably greater magnitude than in other matrixes. The submicrometer capillaries are batch-fabricated on silicon through a fabrication process that does not require high-resolution advanced lithography or well-controlled wafer bonding techniques to define their critical dimension.



The past decade has seen a plethora of engineered micro/nanostructures for the size-dependent electrophoretic separation of macromolecules in free solution, particularly DNA and proteins.^{1–3} Such sieving structures, given their highly regular topography and precise dimensions, have been promoted as a potential substitute for restrictive gelatinous materials (gels) or viscous sieving polymer solutions.

Interest in these so-called artificial gel structures is primarily stimulated by several shortcomings of the conventional sieving matrixes. First, they perform poorly when separating long-stranded DNA molecules (>10 kbp) under a constant electric field.⁴ Pulsing or switching the field extends this limit to 10 Mbp yet leads to highly inefficient separation that takes many hours.^{5–7} This limitation could be overcome with novel restrictive media such as the engineered artificial gels which may present completely new physical effects in probing dynamics of macromolecules. Second, the conventional gels need to be freshly prepared beforehand by a skilled operator and their nontrivial incorporation into confining spaces hinders microchip-based analytical systems. More practical systems could result from the use of artificial gels and their direct integration into microchips within the same batch-fabrication process. Third, with their random arrangement of pores and varying pore sizes, the conventional gels are too complex platforms to allow for a well-controlled experimental study of the sieving mechanism. Precisely controlled dimensions of the engineered artificial gel structures could allow for more rigorous

tests for the existing theories and may lead to more insightful models of electrophoresis.

Since the seminal work of Volkmuth and Austin,⁸ the artificial gel structures have largely presented confining spaces on a structured planar surface under a coverplate of glass or soft elastomer directly bonded over.⁹ The bonding techniques are, however, sensitive to particulate contamination.^{10,11} Alternatively, the artificial gels have been fabricated as a single monolithic unit by removing a sacrificial spacer (polysilicon) between a pair of thin-film structural layers (silicon nitride) placed on a planar substrate (silicon).^{12,13} However, thin films usually suffer from residual stresses and mechanical defects.¹⁴ Typical gel designs included arrays of micrometer^{8,15–17} or submicrometer-scale^{12,13,18–20} pillars (post arrays), asymmetric obstacle courses (Brownian ratchets),^{21–24} or microchannels with alternating segments of deep and shallow regions (slit-well motifs),^{25–30} nearly all patterned via optical (contact or projection) or electron-beam (e-beam) lithography and subsequent dry etching. Post arrays were designed with micrometer-scale gaps (1–2 μm) to extend Ogston sieving regime to long molecules.⁸ Although this was proved to be a challenge under constant electric field due to complex hooking dynamics of molecules, pulsing the field induced a high-speed

Received: October 4, 2013

Accepted: December 3, 2013

Published: December 3, 2013

separation several orders of magnitude faster than by the polymer gels.^{15,16} Later, the approach formed the basis of the “DNA prism”, the device that spatially sorts and retrieves large DNA fragments by size in seconds in continuous operation.^{8,7} Meanwhile, post arrays with submicrometer-scale gaps (500 nm) showed successful separation under a constant electric field with Ogston and reptation-like mechanisms.¹⁹ Further, a novel mechanism, entropic recoil effect, was revealed for long DNA molecules trapped at the interface of a post array with smaller gaps (~ 100 nm) and thereby leading to their separation under a pulsed field.¹³ Entropic effects were also found responsible for the increased escape and higher mobility of longer DNA molecules in the slit-well motif.^{25–28}

Here, a new artificial gel structure is introduced based on a semiconductor fabrication process that does not require advanced patterning tools (e.g., projection, e-beam, or nanoimprint) or meticulous wafer bonding techniques to precisely define the confining spaces. The process rather uses standard photolithography and dry etching techniques to impart a surface topography with coarse trench features ($>1 \mu\text{m}$) which then serves as a template for precision-molding in-plane cylindrical glass capillaries with a submicrometer diameter. The diameter is adjusted through an annealing step in which capillaries evolve into cylindrical tubes and then gradually shrink in diameter while preserving their shape under thermal reflow of glass. The capillaries are self-enclosed owing to a nonconformal deposition profile of the glass film on structured silicon. A similar approach was used by others to demonstrate self-enclosed micro- and nanochannels in silica³¹ and polymer.³² The anneal step subsequently introduced here further led to the shape transformation of such self-enclosed channels into cylindrical capillaries. Previously, the shape transformation via thermal reflow was realized directly on a silicon surface topography to produce self-enclosed nanochannels without depositing any additional material.³³ The process shown here was originally developed for short capillary segments ($<50 \mu\text{m}$) to probe cells in microfluidics^{34–36} but later extended to provide longer segments (>10 mm) capable of electrophoretic separation of amino acids under high electric field (90 kV/m) with negligible Joule heating.³⁷ Very recently, capillaries with a diameter of as small as 50 nm were attained through extended anneal time and shown to effectively stretch λ -phage DNA (λ -DNA).³⁸

The design concept investigated here for DNA sieving characteristics is shown in Figure 1a. It utilizes a traditional sample injection cross-junction for launching DNA plugs into an integrated capillary array. The capillary array, the sieving matrix, adopts the repeated pattern of a slit-well motif where the rectangular slits are replaced by parallel arrangement of identical cylindrical glass capillaries. The submicrometer capillaries maintain a uniform diameter over a length of L_c and then give rise to conical fluid access ports over L_e on either side owing to diverging trench ends in which they are molded (Figure 1b). The spatial gradient profile offered by the fluid access ports would be of value for facilitating long DNA chains (e.g., genomic DNA) to prestretch and thus get more effectively introduced into the capillaries under the applied field strength.³⁹

MATERIALS AND METHODS

Microfabrication. Cylindrical glass capillaries were integrated on silicon through a process previously detailed.³⁷ Precursor for each capillary was defined within a narrow trench

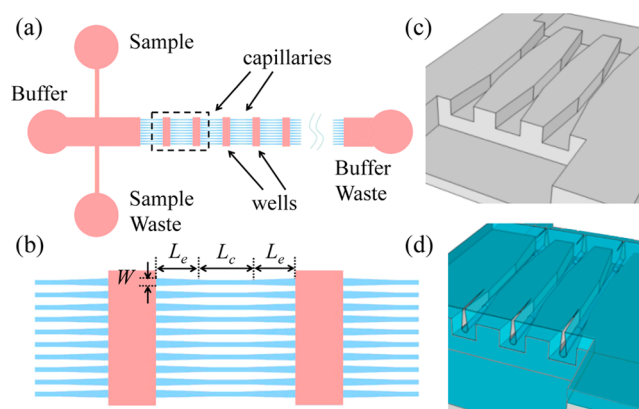


Figure 1. Conceptual illustration of the artificial sieving matrix based on the self-enclosed submicrometer cylindrical glass capillaries. (a) Linearly arranged pattern of capillary-well units along the separation channel integrated with a sample injection cross-junction. (b) A single unit of 10 capillaries (blue) in parallel and flanked by deep wells (red). The capillaries possess a buried center that is uniform over a length of L_c but then gradually expands and opens up over L_e toward the wells. (c and d) 3D rendering of silicon substrate prestructured with a dual-step profile described for a unit of three parallel capillaries (c) before and (d) after doped glass deposition and thermal reflow.

in silicon as a self-enclosed void of a triangular cross-sectional profile upon nonconformal deposition of a doped glass layer. Reflow of the doped glass layer during a thermal anneal step led to shape transformation as the triangular voids evolved into cylindrical capillaries so as to minimize their free surface energy. Along with the cylindrical capillaries, fluid access ports also emerged owing to the unique design of diverging trenches terminating at a larger width at their open ends (Figure 1, parts c and d). This approach eliminated the necessity of dry etching the glass layer to form the access ports, which would be technically cumbersome and compromise the device electrical passivation. Such fabrication strategy has been successfully implemented in our previous work for the microfluidic integration of long cylindrical glass capillaries (10 mm).³⁷ The same process steps were executed here through a new set of masks involving segmented-capillary designs. A dual-step profile was imparted to the substrate by deep reactive ion etching (DRIE) silicon initially through a photoresist mask (to form the wells, reservoirs, and the channels for the sample injection junction up to $23 \mu\text{m}$ deep) and then, after stripping off the resist mask, through a silicon dioxide mask (to form $3.5 \mu\text{m}$ wide and deep trenches). Both masks were consecutively patterned on the substrate before the DRIE steps. The structured wafers were passivated with a thermally grown $0.7 \mu\text{m}$ thin-film silicon dioxide underneath a nonconformal layer of $5 \mu\text{m}$ thick phosphosilicate glass (PSG) through a low-pressure chemical vapor deposition process (LPCVD, 180 mTorr, 420°C). The triangular voids, the so-called capillary precursors, were turned into cylindrical capillaries by having doped glass reflow into the trenches during a thermal anneal step performed at 1000°C for 1 h. Each device was individually aligned and permanently bonded with a plain elastomer slab of poly(dimethylsiloxane) (PDMS; Dow Corning 184) with four inlet/outlet holes as soon as their mating surfaces activated in oxygen plasma (29.6 W for 45 s, Harrick Plasma).

Measurements. All experiments took place on an epifluorescence microscope (FN1, Nikon) equipped with a $10\times/0.3$ NA objective lens (Carl Zeiss) and a diode-pumped solid-

state laser at 473 nm (LSR473NL, Lasever Inc.) replacing the halogen lamp house to effectively induce fluorescence. Individual fluorescent bands of DNA strands were eluted as a result of electrophoretic separation and captured through a CCD camera (RT3Mono, SPOT) mounted on the microscope. DNA was prestained with intercalating dye SYBR Green (Sigma-Aldrich) at a dye-to-base-pair ratio of 1:2.5 and prepared to a final concentration of 50 $\mu\text{g}/\text{mL}$ in 5 \times TBE electrophoresis buffer (450 mM Tris/borate, 10 mM EDTA (ethylenediaminetetraacetic acid), pH 8.3) containing 1% v/v poly(vinylpyrrolidone) (PVP, MW = 10 000) to suppress electroosmotic effect. Each device was loaded prior to introducing DNA sample by placing the electrophoresis buffer in all the reservoirs. Double-stranded DNA (dsDNA) fragments from bacteriophage lambda cI857 Sam7 (λ DNA) along with a mixed digest of *Eco*RI-cut λ -phage DNA (3530–21 226 bp) were all obtained commercially (Sigma-Aldrich), while a 600 bp DNA at the O allele of human ABO blood group gene was amplified by polymerase chain reaction (PCR). Injection and separation of a sample plug was realized with electric fields applied through platinum electrodes (Leego Precision Alloy) immersed in the reservoirs from a high-voltage power supply (Tianjin Dongwen Co. Ltd.). Time-series images were analyzed through an image processing software (ImageJ, NIH, Bethesda), and respective electropherograms were generated based on fluorescence intensities acquired from the region of interest (ROI $\sim 2 \mu\text{m}$ by $2 \mu\text{m}$).

RESULTS AND DISCUSSION

Sieve Structure. Figure 2a shows a section of a representative device, prior to deposition of the doped glass layer, where the separation channel can be seen extending from the sample injection cross-junction. The sample is electrokinetically injected through one of the side channels 20 μm

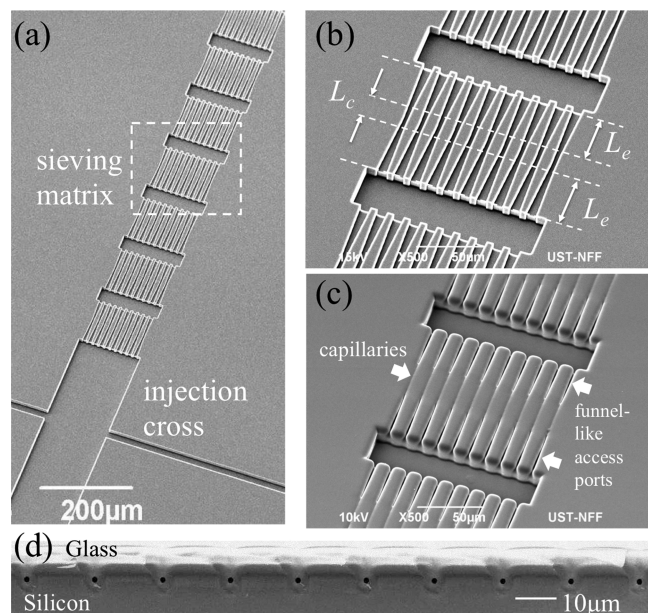


Figure 2. SEM images of a representative device. (a) A section of the sieving matrix near the sample injection junction depicted prior to doped glass deposition (scale bar: 200 μm). (b and c) A single unit shown (b) before and (c) after doped glass deposition and thermal reflow (scale bars: 50 μm). (d) Cross-sectional view of 10 capillaries across a unit (scale bar: 10 μm).

wide and 5 mm long into the separation channel 140 μm wide and 5 mm long. The channel integrates a sieving matrix of capillary segments cascaded 32 units in total (n) and offset 200 μm from the junction. A single unit is flanked by a pair of wells 35 μm long and 140 μm wide as depicted in close-up views before and after deposition and thermal reflow of the doped glass layer in Figure 2, parts b and c. Each unit contains 10 identical cylindrical capillaries self-enclosed in trench segments of a uniform width 3.5 μm and length 10 μm (L_c). The capillaries are accessed via funnel-like ports formed during thermal reflow of doped glass within diverging trench segments over a length of 50 μm (L_e) and terminating at a width (W) of 7 μm . All the wells and channels in this specific design are 13 μm deep, while the trenches are 3.5 μm prior to deposition of the glass layer. The depth varies across the designs along with the length of the uniform trench segment (L_c). Note the highly uniform diameter of the capillaries, 750 nm, achieved through low-resolution photolithography in a standard silicon process (Figure 2d).

Capillary Segment Length. Sieve performance was first evaluated on electrophoretic separation of mixed digests of *Eco*RI-cut λ -phage DNA (3530–21 226 bp) and compared across three designs identical in all features, including the channel/well depth (23 μm), but the uniform capillary length L_c (10, 100, and 200 μm), and hence the total number of units n , cascaded along the 5 mm long separation length (32, 19, and 13). The size of a representative sample DNA plug is shown during a “pinched” injection scheme, migrating toward the anode in the capillary-free region of the separation channel (Figure 3a). Figure 3b shows electropherograms obtained at

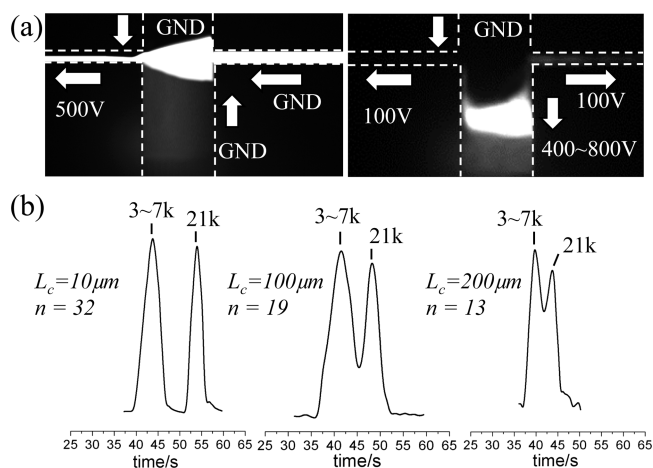


Figure 3. Device characterization. (a) Fluorescence micrographs showing “pinched” injection of a DNA sample plug. (b) Electropherograms obtained at the end of 5 mm long separation channels in three distinct devices. The devices were identical in channel/well depth (23 μm), but the uniform capillary length L_c and the total number of units n were as labeled in the plots. Separation electric field strength: 1.6 kV/cm.

the detection point approximately 5 mm downstream of the injection cross-junction at an average field of 1.6 kV/cm. As can be seen, through the device with 10 μm long capillaries, the DNA fragments were resolved into two separate bands in less than a minute. With a radius of gyration ($R_g \sim 345 \text{ nm}$ for 21 kbp) smaller than the capillary diameter, the fragments elute in ascending order of chain length on the basis of Ogston sieving.⁴ Accordingly, the peak eluted last belongs to the longest chain

length (21 kbp), while the faster peak contains all the smaller fragments that could not be resolved within the given separation length (3.5, 4.8, 5.6, 5.8, and 7.4 kbp). This has been verified also through experiments whereby sample plugs of homogeneous chains were independently electrophoresed through the device and the smaller chain size (600 bp) was repeatedly found eluting out earlier than intact λ -DNA (48.5 kbp).

From the electropherograms, one can notice that the resolving power deteriorates, as the capillaries get longer and a less number of units can be packed along the same separation length. For each device, the resolution, $R_s = 2\Delta t/(W_1 + W_2)$, which is the distance between the two peaks scaled by their average width at base, is listed in Table 1. A 10-fold increase in

Table 1. Device Specifications and Separation Metrics Pertaining to the Plots (Figure 3b)

specifications			performance	
L_c (μm)	n	$n \times L_c$ (μm)	R_s	N_t ($\times 10^3$)
10	32	310	1.34	2.39 ^a
100	19	1900	0.96	1.40 ^a
200	13	2600	0.79	1.43 ^a

^aAccording to the peak representative of 21 kbp chains in Figure 3b.

the capillary length L_c to 100 μm reduces the resolution below a critical value of 1, while a further increase to 200 μm makes the two peaks barely resolvable ($R_s = 0.79$). Overall, the cumulative capillary length that the fragments have to go through is increased from 310 to 2600 μm while the number of units is reduced from 32 to 13. This suggests that DNA sieving mainly occurs at the capillary-well interface (entropic barrier) rather than capillary interior. A similar trend was also reported for the slit-well motif but using far more units (>1000) and lower average fields (<100 V/cm) than here.^{25–30} Typical values for the theoretical plate number N_t of the capillary matrix are in the order of 10^3 and also decline with the increased capillary length L_c as listed in Table 1.

Characteristic Threshold Voltage. An interesting encounter in our device is that the band launching through the capillary units could not be achieved below a critical threshold voltage, which occurs at a far greater magnitude than those reported for the slit-well motifs. Specifically, in the devices described above (Figure 3), values below 800 V were found to be insufficient to drive most of the fragments through the first unit regardless of the duration being applied. This could be mainly attributed to the fact that majority of the applied voltage falls across the capillaries, given their extremely high electrical resistance, leaving the wells behind with a fairly low electric field (<3 V/cm for below 800 V). Such field threshold (~ 3 V/cm) fares well with those in the slit-well structure of a comparable separation length that is, however, subjected to tens of volts only. Meanwhile, field intensity within the capillaries (~ 2 kV/cm at 800 V) is at least an order of magnitude higher than within the slits (~ 150 V/cm at 120 V applied over 15 mm).²⁷

Well Depth. Local field intensity can be further enhanced through a reduced well depth so as to attain a lower threshold voltage. Threshold voltage for the band launching, for instance, across the designs with 10 μm long capillaries, 5 mm long separation channel, and a well depth of 23, 13, 8, and 3 μm was identified to be near 800, 400, 300, and 150 V, respectively. With a well depth of 13 μm , 500 V was sufficient to launch

DNA chains into two separate bands, Figure 4a, slightly better in $R_s = 1.98$ and $N_t = 3.4 \times 10^3$ than through the same design

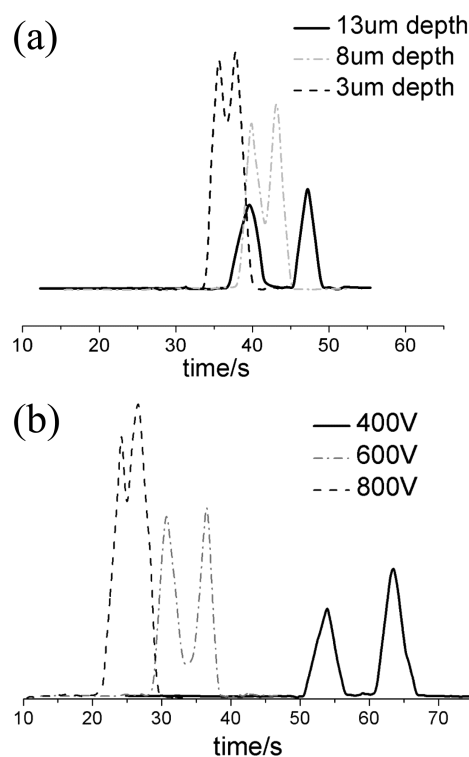


Figure 4. Electropherograms from the devices that are identical but either with (a) varying channel/well depth and subjected to a fixed electric field strength at 1 kV/cm or with (b) a fixed channel/well depth of 13 μm but subjected to varying electric field strengths. In all, $L_c = 10$ μm and $n = 32$ along the separation length of 5 mm.

with a well depth of 23 μm . A slight increase in the migration speed was also noticed. A further reduction in the well depth continued to increase the migration speed and enhance the theoretical plate number but also deteriorated the resolution. This is in contrast with the slit-well design where a reduced well depth caused an increase in the separation selectivity during entropic trapping regime owing to the subsequent reduction in the slit electric field and thus the escape probability of the molecules.²⁸ In our devices, however, theory suggests that the capillary electric field hardly changes ($<0.5\%$ at 1.4 kV/cm) while the field in the wells proportionally increases from 2 to 15 V/cm in response to ~ 7 -fold reduction in the well depth. While such field increase led to a slightly faster migration speed, it compromised separation selectivity because of its more profound impact on the large molecules (21 kbp) than those smaller. This rather concurs with the field-dependent electrophoretic mobility of molecules observed with the slit-well configuration during the Ogston sieving regime,^{29,30} which reportedly influences the larger molecules more.

Separation Voltage. A similar trend was also noticed when the field increase originated from a surge in voltage intensity provided that the voltage applied across the separation channel was above the threshold. For instance, on the design with a fixed well depth of 13 μm , both the peaks increased migration rate by ~ 1.75 -fold, responding more or less equally to a level rise from 400 to 600 V (Figure 4b). From 600 to 800 V, a somewhat higher mobility, however, was unveiled by the large chains (21 kbp). This might be explained by the fact that the

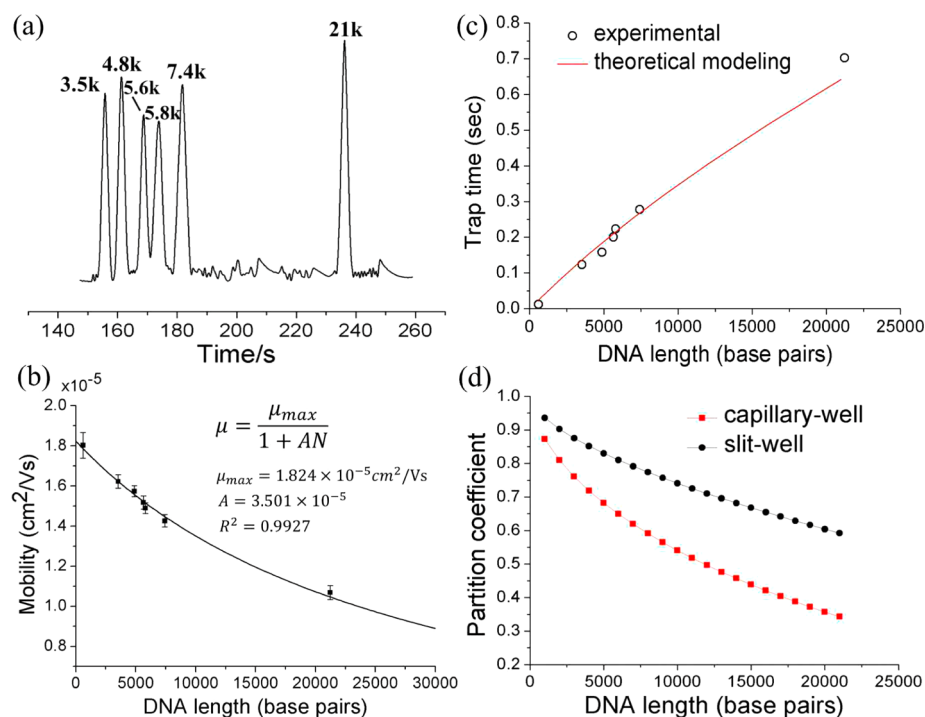


Figure 5. (a) Electropherogram obtained at the end of a 20 mm long separation channel having $n = 128$, $L_c = 10 \mu\text{m}$, and the channel/well depth of $13 \mu\text{m}$. Separation electric field strength: 800 V/cm . (b and c) DNA mobility and the mean trapping time τ_{trap} in the same matrix as a function of the chain length (600 bp to 21 kbp). (b) The error bars indicate the standard errors of the respective mean values (the symbols) for five repetitious runs on the same device. (c) The symbols indicate the values obtained from eq 1 using the measured average mobility and μ_{max} . The curve is based on eq 2 with the fitting parameter $\alpha = 2.5 \times 10^5 \text{ V}^2 \text{ s}/(\text{m}^2 \text{ bp})$. (d) Partition coefficient values as a function of the size of the chain length calculated for the capillary matrix and equivalent slit-well motif (see the Supporting Information).

field strength within the well structures must reach a critical level to become more effective on the large chains. It should be noted that the projected field strengths within the well structures, 4 and 5.4 V/cm at 600 and 800 V , respectively, remain far below 15 V/cm , the field strength reachable at a lesser voltage (500 V) when the well depth is $3 \mu\text{m}$ (Figure 4a). Therefore, the dramatic increase observed in the overall migration rate must result primarily from an increased capillary electric field (2.3 kV/cm at 800 V) typically ~ 1.6 -fold of those reported in Figure 4a.

Separation Length. To further resolve the smaller fragments within the first-eluted band, the separation length was increased by a factor of 4 on the design with $10 \mu\text{m}$ long capillaries and a fixed well depth of $13 \mu\text{m}$. This led to a 4-fold increase in the number of capillary units to $n = 128$ cascaded along the separation length 20 mm . At the threshold field, 800 V/cm , the smaller fragments were successfully separated from the larger chains (21 kbp) being completely resolved within only 4 min as shown in Figure 5a. The bands 5.6 and 5.8 kbp, although being very close, were still resolvable ($R_s = 1.23$) within the extended length. Also, an order of magnitude increase in the theoretical plate numbers $2.3\text{--}6 \times 10^4$ plates ($1.2\text{--}3 \times 10^6$ plates/m) was noted in comparison to those in Figure 3b. These values are on par with those from the state-of-the-art sieving matrixes at comparable lengths and yet achieved here at a fraction of their time.^{19,27} This can be attributed to that the equilibrium-sieving mode can be sustained in our structure at a much greater average field. The short fragments were observed to resolve, although not fully, even at the separation length of 10 mm ($n = 64$) (Figure S-1, Supporting Information).

Electrophoretic Mobility. Figure 5b reveals the mobility data derived from the DNA band elution time, the migration distance, and the applied electric field. The data also includes the mobility value for the smaller chains (600 bp) independently electrophoresed in the same design through which *EcoRI*-cut λ -DNA fragments were separated. Fitting to a model where the mobility $\mu = \mu_{\text{max}}/(1 + AN)$ is expressed in terms of the number of base pairs N and two fitting parameters μ_{max} and A ³⁰ showed excellent agreement for a specific combination of $\mu_{\text{max}} = 1.82 \times 10^{-5} \text{ cm}^2/(\text{V s})$ and $A = 3.5 \times 10^{-5}$ ($R^2 = 0.993$). The former is the maximum sieving-free mobility inside the design, whereas the latter is inversely related to the average electric field E_{av} along with the sieve geometry including the unit length L_w , and partition coefficient K according to the equilibrium partitioning theory and Kramer's theory (see below).³⁰ It should be noted that the slope of the mobility curve $d\mu/dN$ is an increasing function of A and rather significant as it determines the size selectivity of the design.²⁹ A greater size selectivity occurs with a large A and thus requires that the term $L_w E_{\text{av}} K$ be kept at a minimum.

Mean Trapping Time. The DNA fragments migrating through the capillary matrix spends on average a finite lifetime at a capillary entrance (entropic barrier). The mean trapping time τ_{trap} can be inferred from the experimental mobility values through the following relation:

$$\mu = \frac{\mu_{\text{max}}}{1 + \tau_{\text{trap}}/\tau_m} \quad (1)$$

where $\tau_m = L_w/\mu_{\text{max}} E_{\text{av}}$ refers to the drift time of the molecules between the consecutive traps. Figure 5c shows the values calculated based on the mean experimental mobility and

compares them to a curve obtained from the kinetic model based upon the equilibrium partitioning theory and Kramer's rate theory:³⁰

$$\tau_{\text{trap}} = \frac{\alpha N}{E_{\text{av}}^2 K} e^{-\varepsilon} \quad (2)$$

where α is the fitting parameter, K is the partition coefficient of the capillary-well matrix described in Figure Sd (details in the Supporting Information), and $\varepsilon = \Delta W/k_B T$ is the reduced potential with ΔW being the electrical potential energy drop in the translation of molecules over the entropic barrier along the field direction, k_B being the Boltzmann's constant, and T being the absolute temperature. The electrical potential energy drop can be approximated as

$$\Delta W = NqE_w d_r \quad (3)$$

where q is the effective charge per base pairs, 2.49×10^{-21} C/bp,³⁰ E_w is the electric field within the wells, and $d_r = (Dt_w)^{1/2}$ is the transition region radius given by the characteristic diffusion length of the molecules ($D \sim N^{-0.6}$ being the diffusion coefficient of the molecules⁴⁰ and $t_w = L_w/\mu_{\text{max}}E_{\text{av}}$ being the average time it takes for the molecules to cross the well length L_w).

The theoretical curve agrees well with the experimentally derived τ_{trap} values (Figure 5c). The slight deviations could be attributed to the non-negligible internal conformations and rotational states of the coiled chains in the kinetics of overcoming the entropic barriers. It should be highlighted that eqs 1 and 2 can be combined to obtain the mobility fitting parameter:

$$A = \mu_{\text{max}} \alpha e^{-\varepsilon} / L_w E_{\text{av}} K$$

In Comparison to the Slit-Well Motif. Ogston sieving mechanism in the slit-well structure breaks down at high fields (100 V/cm) with an inevitable loss of resolution for rodlike DNA.³⁰ Lowering the field could recover the selectivity (A) but would also cause a great delay in migration time; sieving 100 bp DNA ladder takes about 3 h to complete at ~ 26 V/cm.³⁰ Considering the size of the chains separated here (several thousands base pairs) and the critical sieve dimension (750 nm), a direct comparison is made with theoretical predictions from eqs 1 and 2 for an equivalent slit-well model upon replacing the capillary segments with slits 750 nm deep, 140 μm wide, and 110 μm long in the design associated with Figure 5. In such a slit-well model subjected to a high field strength ($E_{\text{av}} = 800$ V/cm), the mean trapping time τ_{trap} is found to be extremely small in the order of hundreds of nanoseconds, negligible in comparison to $\tau_m \sim 1$ s. Thus, the mobility is nearly constant, $\mu \sim \mu_{\text{max}}$ independent of N , implying no separation (the size selectivity $A = 4 \times 10^{-11}$).

The mean trapping time of the chains by the slits is suggested to be 6 orders of magnitude shorter than those by the capillaries (hundreds of milliseconds). This cannot be simply explained by the partition coefficient K . As shown in Figure 5d, K is expectedly smaller in the capillary-well configuration than in the slit-well motif and decays faster with the chain length (derivation in the Supporting Information). Yet, the deviation in K values does not grow apart more than an order of magnitude even for the largest chains. The fitting parameter α for the two geometries is not expected to vary greatly as it is predominantly determined by the diffusivity of the chains.⁴¹ The exponential term $e^{-\varepsilon}$, however, renders variations in the

reduced potential ($\varepsilon = \Delta W/k_B T$) far more significant. In the capillary matrix, ε remains less than 1 ($\varepsilon \sim 0.5$) based on $\Delta W \sim k_B T$, whereas in the slit-well configuration ΔW is at least an order of magnitude larger than $k_B T$, hence, $\varepsilon > 10$. Such variation in ε is sufficient to account for the suggested differences in τ_{trap} . A higher ΔW prevails in the slit-well motif than in the capillary-well matrix as the field strength E_w in the former quickly climbs up with the applied voltage (64 V/cm as opposed to 2.6 V/cm).

Simulations^{42–44} and experiments⁴⁵ performed on the slit-well design, however, revealed a nonequilibrium sieving mode beyond the Ogston breakdown where higher fields help separation recover but with a reversed elution order of bands and a speed 1–2 orders of magnitude faster than with Ogston sieving at lower fields. Still, the selectivity is compromised as compared to the Ogston sieving regime.⁴⁵ A highly restrictive sieve structure, like the capillaries here, sustains differential migration of chains at higher fields without compromising the selectivity or Ogston equilibrium, thereby achieving a fast separation. Inside a capillary, the configurational freedom of molecules is limited to a quasi-one-dimensional space (smaller partition coefficient, K , and thus greater entropic energy barrier $-k_B T \ln K$). More importantly, the capillaries impose a higher electrical resistance, limiting the field strength inside the wells to a small fraction (<1%) of the average field even at high operating voltages applied for a fast separation. This ensures that the driving electrical potential energies commensurate with the entropic barriers such that the separation takes place near equilibrium for an optimum resolving power.

CONCLUSION

The novel matrix structure disclosed herein with a fast sieving characteristic may lead to future integrated nucleic acid analyses systems that are compact, fast, and more practical. The structure could be further optimized for a range of applications. For instance, the capillary diameter can be tailored through anneal time and temperature for sieving shorter or longer DNA chains as well as specific proteins. The smallest diameter evaluated to date (150 nm) in our design with λ -DNA ($R_g \sim 520$ nm) revealed the crossover from Ogston-like sieving to entropic trapping (Figure S-2, Supporting Information). Investigations are currently underway for sieving matrixes with the capillary diameter less than 100 nm.

ASSOCIATED CONTENT

Supporting Information

Additional information as noted in text. This material is available free of charge via the Internet at <http://pubs.acs.org>.

AUTHOR INFORMATION

Corresponding Author

*Phone: +852-2358 7068. Fax: +852-2358 1485. E-mail: eelyobas@ust.hk.

Notes

The authors declare no competing financial interest.

ACKNOWLEDGMENTS

This project was financially supported in part by the Startup Grant from the Electronic and Computer Engineering Department, HKUST, and the Research Project Competition Grant by the HKUST (Grant No. RPC11EG09).

■ REFERENCES

- (1) Dorfman, K. D. *Rev. Mod. Phys.* **2010**, *82*, 2903–2947.
- (2) Salieb-Beugelaar, G. B.; Dorfman, K. D.; van den Berg, A.; Eijkel, J. C. T. *Lab Chip* **2009**, *9*, 2508–2523.
- (3) Fu, J.; Mao, P.; Han, J. *Trends Biotechnol.* **2008**, *26*, 311–320.
- (4) Viovy, J.-L. *Rev. Mod. Phys.* **2000**, *72*, 813–872.
- (5) Schwartz, D. C.; Cantor, C. R. *Cell* **1984**, *37*, 67–75.
- (6) Carle, G. F.; Frank, M.; Olson, M. V. *Science* **1986**, *232*, 65–68.
- (7) Chu, G.; Vollrath, D.; Davis, R. W. *Science* **1986**, *234*, 1582–1585.
- (8) Volkmuth, W. D.; Austin, R. H. *Nature* **1992**, *358*, 600–602.
- (9) Mao, P.; Han, J. *Lab Chip* **2005**, *5*, 837–844.
- (10) Fan, Z. H.; Harrison, D. J. *Anal. Chem.* **1994**, *66*, 177–184.
- (11) Jacobson, S. J.; Moore, A. W.; Ramsey, J. M. *Anal. Chem.* **1995**, *67*, 2059–2063.
- (12) Turner, S. W.; Perez, A. M.; Lopez, A.; Craighead, H. G. *J. Vac. Sci. Technol., B* **1998**, *16*, 3835–3840.
- (13) Cabodi, M.; Turner, S. W. P.; Craighead, H. G. *Anal. Chem.* **2002**, *74*, 5169–5174.
- (14) Stern, M. B.; Geis, M. W.; Curtin, J. E. *J. Vac. Sci. Technol., B* **1997**, *15*, 2887–2891.
- (15) Duke, T. A. J.; Austin, R. H.; Cox, E. C.; Chan, S. S. *Electrophoresis* **1996**, *17*, 1075–1079.
- (16) Bakajin, O.; Duke, T. A. J.; Tegenfeldt, J.; Chou, C. F.; Chan, S. S.; Austin, R. H.; Cox, E. C. *Anal. Chem.* **2001**, *73*, 6053–6056.
- (17) Huang, L. R.; Tegenfeldt, J. O.; Kraeft, J. J.; Sturm, J. C.; Austin, R. H.; Cox, E. C. *Nat. Biotechnol.* **2002**, *20*, 1048–1051.
- (18) Baba, M.; Sano, T.; Iguchi, N.; Iida, K.; Sakamoto, T.; Kawaura, H. *Appl. Phys. Lett.* **2003**, *83*, 1468–1470.
- (19) Kaji, N.; Tezuka, Y.; Takamura, Y.; Ueda, M.; Nishimoto, T.; Nakanishi, H.; Horiike, Y.; Baba, Y. *Anal. Chem.* **2004**, *76*, 15–22.
- (20) Chan, Y. C.; Lee, Y.-K.; Zohar, Y. J. *Micromech. Microeng.* **2006**, *16*, 699–707.
- (21) Duke, T. A. J.; Austin, R. H. *Phys. Rev. Lett.* **1998**, *80*, 1552–1555.
- (22) Ertas, D. *Phys. Rev. Lett.* **1998**, *80*, 1548–1551.
- (23) van Oudenaarden, A.; Boxer, S. G. *Science* **1999**, *285*, 1046–1048.
- (24) Huang, L. R.; Cox, E. C.; Austin, R. H.; Sturm, J. C. *Anal. Chem.* **2003**, *75*, 6963–6967.
- (25) Han, J.; Craighead, H. G. *J. Vac. Sci. Technol., A* **1999**, *17*, 2142–2147.
- (26) Han, J.; Turner, S. W.; Craighead, H. G. *Phys. Rev. Lett.* **1999**, *83*, 1688–1691.
- (27) Han, J.; Craighead, H. G. *Science* **2000**, *288*, 1026–1029.
- (28) Han, J.; Craighead, H. G. *Anal. Chem.* **2002**, *74*, 394–401.
- (29) Fu, J. P.; Mao, P.; Han, J. Y. *Appl. Phys. Lett.* **2005**, *87*, 263902.
- (30) Fu, J. P.; Yoo, J.; Han, J. Y. *Phys. Rev. Lett.* **2006**, *97*, 018103.
- (31) Cao, H.; Yu, Z.; Wang, J.; Tegenfeldt, J. O.; Austin, R. H.; Chen, E.; Wu, W.; Chou, S. Y. *Appl. Phys. Lett.* **2002**, *81*, 174–176.
- (32) Ilic, B.; Czaplowski, D.; Zhalaludinov, M.; Schmidt, B.; Craighead, H. G. *J. Vac. Sci. Technol., A* **2002**, *20*, 2459–2465.
- (33) Xia, Q.; Morton, K. J.; Austin, R. H.; Chou, S. Y. *Nano Lett.* **2008**, *8*, 3830–3833.
- (34) Ong, W.-L.; Kee, J.-S.; Ajay, A.; Ranganathan, N.; Tang, K.-C.; Yobas, L. *Appl. Phys. Lett.* **2006**, *89*, 093902.
- (35) Ong, W.-L.; Tang, K.-C.; Agarwal, A.; Nagarajan, R.; Luo, L.-W.; Yobas, L. *Lab Chip* **2007**, *7*, 1357–1366.
- (36) Tang, K.-C.; Reboud, J.; Kwok, Y. L.; Peng, S. L.; Yobas, L. *Lab Chip* **2010**, *10*, 1044–1050.
- (37) Cao, Z.; Ren, K. N.; Wu, H. K.; Yobas, L. *Biomicrofluidics* **2012**, *6*, 036501.
- (38) Liu, Y.; Yobas, L. *Biomicrofluidics* **2012**, *6*, 046502.
- (39) Cao, H.; Tegenfeldt, J. O.; Austin, R. H.; Chou, S. Y. *Appl. Phys. Lett.* **2002**, *81*, 3058–3060.
- (40) Smith, D. E.; Perkins, T. T.; Chu, S. *Macromolecules* **1996**, *29*, 1372.
- (41) Ajdari, A.; Prost, J. *Proc. Natl. Acad. Sci. U.S.A.* **1991**, *88*, 4468.
- (42) Streek, M.; Schmid, F.; Duong, T. T.; Ros, A. J. *Biotechnol.* **2004**, *112*, 79–89.
- (43) Cheng, K. L.; Sheng, Y. J.; Jiang, S. Y.; Tsao, H. K. *J. Chem. Phys.* **2008**, *128*, 101101.
- (44) Laachij, N.; Declet, C.; Matson, C.; Dorfman, K. D. *Phys. Rev. Lett.* **2007**, *98*, 098106.
- (45) Strychalski, E. A.; Lau, H. W.; Archer, L. A. *J. Appl. Phys.* **2009**, *106*, 024915.